applied sciences

MDPI

Article

Thermal Relaxation Spectra for Evaluating Luminescence Quantum Efficiency of CASN:Eu^{2+} Measured by Balanced-Detection Sagnac-Interferometer Photothermal Deflection Spectroscopy

Hiromichi Chima [1], Naoyuki Shiokawa [1], Keisuke Seto [1], Kohsei Takahashi [2], Naoto Hirosaki [2], Takayoshi Kobayashi [1,3,4] and Eiji Tokunaga [1,*]

1 Department of Physics, Faculty of Science, Tokyo University of Science, 1-3 Kagurazaka, Shinjuku-ku, Tokyo 162-8601, Japan; 1218532@ed.tus.ac.jp (H.C.); 1213704@alumni.tus.ac.jp (N.S.); seto@rs.tus.ac.jp (K.S.); kobayashi1901@gmail.com (T.K.)

2 Sialon Group, National Institute for Materials Science, 1-1 Namiki, Tsukuba 305-0044, Japan; takahashi.kohsei@nims.go.jp (K.T.); hirosaki.naoto@nims.go.jp (N.H.)

3 Advanced Ultrafast Laser Research Center and Brain Science Inspired Life Support Research Center, The University of Electro-Communications, 1-5-1 Chofugaoka, Chofu, Tokyo 182-8585, Japan

4 Advanced Ultrafast Laser Research Center, Department of Electrophysics, National Chiao-Tung University, 1001 Ta Hsinchu Rd., Hsinchu 300, Taiwan

* Correspondence: eiji@rs.tus.ac.jp; Tel.: +81-3-5228-8214

Received: 26 December 2019; Accepted: 29 January 2020; Published: 4 February 2020

Featured Application: Light energy conversion efficiency can be evaluated for any of the phosphors, solar cells, and plants.

Abstract: Highly sensitive broadband photothermal spectroscopy with a white-light lamp as the excitation source was developed by combining a Sagnac interferometer and balanced detection with a photothermal deflection method. A probe beam was split by a birefringent crystal $CaCO_3$ into signal and reference beams with a balanced intensity. This balanced detection enabled the measurement of photoexcited thermal relaxation spectra of materials in the air over the whole visible range in the weak excitation limit 50 $\mu W/cm^2$. The photothermal excitation spectrum of Eu^{2+}-doped $CaAlSiN_3$ phosphors (CASN:Eu^{2+}) with a high luminescent quantum efficiency was measured to be distinctly different from the photoluminescence excitation spectrum which reflects the absorption spectrum, revealing the thermal relaxation mechanism of the phosphor. Assuming a typical non-radiative relaxation from the higher excited states to the lowest excited state and successively to the ground state, it is demonstrated that the photoluminescence efficiency of the phosphors is readily evaluated simply by comparing the photothermal and photoluminescence excitation spectra.

Keywords: photothermal deflection spectroscopy; Sagnac interferometer; CASN:Eu^{2+}; luminescence quantum efficiency; photothermal excitation spectrum; photoluminescence excitation spectrum; thermal relaxation spectrum; balanced detection; birefringent crystal $CaCO_3$; thermal diffusion length

1. Introduction

In general, measurement of the light energy conversion efficiency in a phosphor, a solar cell, or a plant is not easy technically even though the principle is very simple, because it requires accurate measurement [1] of irradiation light intensity and absorption efficiency (input power), total light

emission energy, generated electric power, or metabolite yield (output power). As demonstrated in this paper, by contrast, if the photothermal spectrum can be measured over a wide spectral range showing the difference in shape from the absorption spectrum, the light energy conversion efficiency can be evaluated based on physically reasonable assumptions about thermal relaxation.

For most substances (especially condensed matter) excluding atoms in a vacuum, most of the excitation energy relaxation rate is dominated by a non-radiative thermal relaxation rate, where the energy is finally released as heat to the surroundings of the sample. As a method for measuring this heat generation, photothermal spectroscopy including photoacoustic spectroscopy has been carried out for a long time. Since the photothermal spectrum is a measure of the heat generation rather than the luminescence amount as a function of the excitation light wavelength, it will be referred to as the photothermal excitation spectrum (PTES) in the rest of this paper as a counterpart of the photoluminescence excitation spectrum (PLES). The advantage of PTES over PLES is that it can be applied to all samples because any material has a non-radiative relaxation process, which is the main relaxation process for most substances except highly fluorescent material. Relaxation between the higher excited states is dominated by a non-radiative thermal relaxation, while relaxation from the lowest excited state to the ground state is characterized by the increased apparent photoluminescence rate including both radiative and non-radiative rates k(apparent) = k(radiative) + k(non-radiative). Thus, information of relaxation paths is obtained by comparing PTES with the absorption spectrum or PLES. To emphasize this feature, PTES is also called the thermal relaxation spectrum in this paper.

However, in the long history of photothermal spectroscopy including photoacoustic spectroscopy, this capability of PTES has not been fully explored. Although there are many pioneering studies that have evaluated various quantum yields (luminescence, metabolite, or triplet-state formation via intersystem crossing) with these spectroscopic methods [2–7] there are only a few examples [4] of PTES with a clear difference from PLES. One of the reasons is that thermal detection is less sensitive than luminescence detection, so that a laser is often used as an excitation light source, making it difficult to measure photothermal spectra over a wide wavelength region. Another reason is that highly luminescent material, which is expected to show a photothermal spectrum clearly different from the absorption spectrum, has a low heat-generation efficiency to make it difficult to obtain the photothermal spectrum.

The difference between the photothermal spectrum and absorption spectrum is expected to be relevant to the relaxation mechanism. Important examples may be in biological systems. For example, this kind of process may be taking place in higher plants: Excessive light energy causes damage to the photosynthetic system, so that excess energy is dissipated by heat dissipation process for the photosynthetic mechanism to be protected. Such a dissipation process is important in nature where the environment changes, known as non-photochemical quenching [8]. Since this heat dissipation process is known to work even with the excitation intensity as weak as 5 mW/cm^2 @ 680 nm, it is necessary to measure the photothermal spectrum in the weak excitation limit for acquisition of the thermal relaxation spectrum reflecting the quantum efficiency of photosynthesis. In the past, however, the photothermal spectrum of a leaf has not been measured with sufficiently weak excitation, and an apparent difference between the photothermal and the absorption spectra has never been observed [5].

In photothermal deflection spectroscopy (PDS), representative of photothermal conversion spectroscopy because it is said that PDS is by one order of magnitude more sensitive than photoacoustic spectroscopy (PAS) [9], a laser is generally used as an excitation light source, and a sample is immersed in a medium having a large temperature coefficient of the refractive index (dn/dT) as the surrounding deflection medium, such as carbon tetrachloride. When a bright white light source such as a Xe lamp is used, the wavelength is often selected by a narrow band filter instead of a diffraction grating spectrometer having a low throughput. The typical spectral excitation light intensity in that case is 1 nW/μm^2 = 0.1 W/cm^2.

Since photothermal deflection spectroscopy detects heat generation accompanying non-radiative relaxation after light absorption of a specimen, many researches have been carried out since the analysis

of its physical properties can be carried out non-destructively irrespective of the morphology of the specimen. Previously we developed the Sagnac-interferometer photothermal deflection spectroscopy (SIPDS) to improve the signal to noise ratio (S/N) by one order of magnitude (detectable temperature change 6×10^{-5} K) [10,11] compared with the original report on PDS [12]. As a result, measurement of broadband photothermal spectra is realized in the air by excitation with a weak narrow-spectrum light from a white-light lamp through a monochromator. The photothermal spectrum is equivalent to the absorption spectrum if 100% of the excitation energy is nonradiatively relaxed, but if it is converted to photoluminescence and/or chemical reaction energies, it becomes different from the absorption spectrum. The difference enables us to evaluate the quantum efficiency of luminescence or chemical energy conversion.

In this paper, we have implemented balanced detection into SIPDS and achieved fourfold improvement in S/N compared with SIPDS without balanced detection. We have applied this system to the measurement of photothermal excitation spectrum (PTES) of Eu^{2+}-doped $CaAlSiN_3$ phosphors [13,14] and estimated the luminescence quantum efficiency solely from comparison with the photoluminescence excitation spectrum (PLES), in good agreement with that measured independently by the absolute quantum efficiency measurement system using integrating sphere [15].

2. Materials and Methods

The details of the experimental methods and detection principle are described in References [10,11]. It was previously shown that the dominant factor of the residual noise in the SIPDS system was linearly correlated with the probe laser beam intensity in Reference [11], where it is suggested that subtractive detection of the probe light should be implemented for further reducing the noise in the system. In the present paper, therefore, we have tested two experimental setups for balanced detection of the probe. For splitting the probe into signal and reference beams, one uses a conventional cube beam splitter (method 1) and the other uses a birefringent crystal (calcite) (method 2). The sample used for comparison of S/N is activated carbon. All the experiments were performed at room temperature.

2.1. Method 1

A cube beam splitter (BS) and a mirror were put before the Sagnac interferometer, as illustrated in Figure 1. The probe laser beam from a He-Ne laser (R-32734, Newport, Irvine, CA, USA) was divided with the beam splitter into the two equal-intensity beams used as the signal and reference beams. The signal beam is transmitted through the refractive index gradient while the reference beam is bypassing it. The interference of both probe and reference laser beams was detected at the same time with two photodiodes after the Sagnac interferometer on the two conditions with/without the excitation light. The signal beam contains information of both the photothermal effect of the sample and the noise factor of the probe laser beam. The reference beam carries only the noise factor common to the probe laser beam. The two photodiodes were connected in the opposite directions to subtract the photocurrent of the reference beam from that of the signal beam. Thus, the residual output signal from the two combined photodiodes carries only the photothermal signal without the probe beam noise. The photocurrent generated from the two photodiodes was input to the lock-in amplifier (7265, Signal Recovery, Edinburgh, UK). Subtraction of the common noise from the probe laser beam was thus successfully performed to achieve the improvement in the S/N of the photothermal deflection detection.

The interference light intensities of the signal and reference beams were adjusted to the same intensity to subtract the noise of the probe laser beam. These two probe laser beams were propagating in parallel via adjusted mirror angle before the BS.

The focal length of the plano-convex lens at the input of the interferometer was 300 mm in both method 1 and 2. The beam waist at the sample was calculated to be 166 μm from the diameter 1.4 mm at the lens, the lens focal length, and the wavelength of He-Ne laser. The modulation frequency of the excitation light was 20.0 Hz.

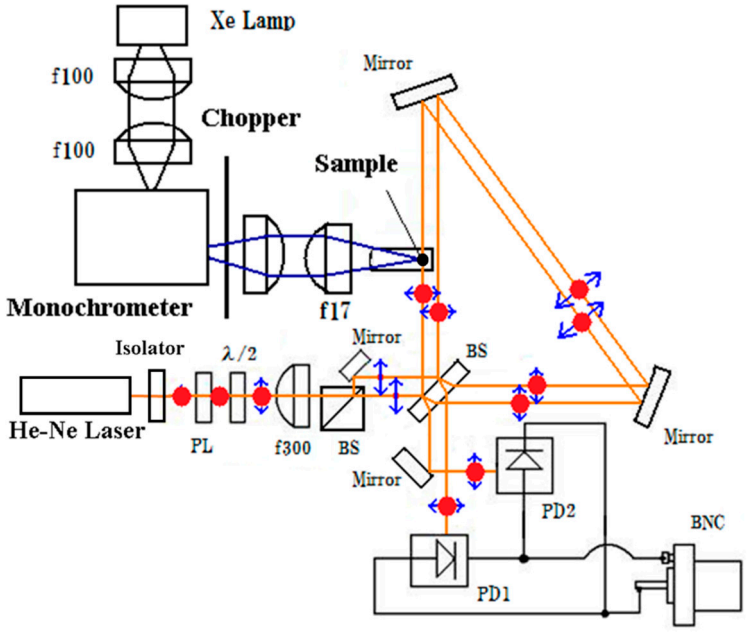

Figure 1. Schematic diagram of the intensity-balance Sagnac interferometer photothermal deflection spectroscopy. The beam splitter (BS) and mirror were inserted before the Sagnac interferometer. These optical components generated two probe laser beams, the signal and reference. The beam diameter was 1.4 mm at the lens and the lateral distance between the two beams was about 5 mm.

2.2. Method 2

In this experiment, a birefringent crystal $CaCO_3$ of $15 \times 15 \times 5$ mm^3 was used to generate the signal beam and reference beam in a parallel direction to each other, as illustrated in Figure 2. The $CaCO_3$ is a uniaxial crystal. If the incidence beam is polarized at 45 degree against the crystal axis of $CaCO_3$, it was split into two equal-intensity beams. The two beams were passed through the common surface of the crystal. Therefore, the two beams were completely aligned parallel and of equal intensity to each other. Then, one of the beams was used as the signal beam to pass the refractive index gradient position while the other beam was used as the reference beam. The signal intensities of interfering light detected by the two photodiodes were adjusted to be equal by appropriate rotation of the polarization angle after the intensity adjustment. This optical system could more effectively reduce the intensity noise of the probe laser beam by subtraction. Further improvement of the S/N was achieved by this optical system designed for complete subtraction of the probe laser beam noise.

The birefringent crystal $CaCO_3$ was placed before the Sagnac interferometer. The wave plate was rotated by 22.5 degrees to make the polarization angle 45 degrees against the $CaCO_3$ crystal axis. By the process the two beam intensities split by the $CaCO_3$ crystal was equalized. These beams were detected with the two photodiodes. The photocurrent generated by two photodiodes was introduced to the lock-in amplifier.

The set-up procedure is explained in detail. The interference light intensity of the two beams were detected with the two photodiodes. The output of two photodiodes was processed by the lock-in amplifier. The sensitivity of the lock-in amplifier was set to 1 μA and the subtractive output from the two photodiodes was adjusted to less than 50 nA compared with the interference light intensity about 8.0 μA.

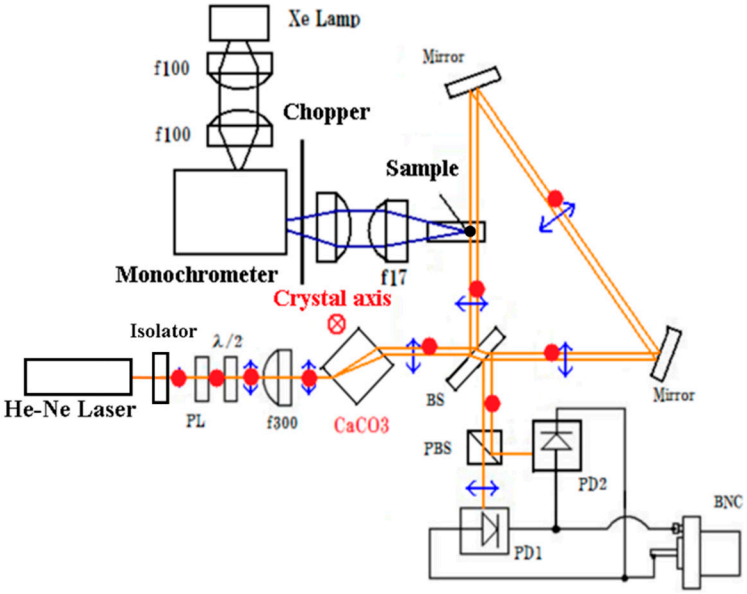

Figure 2. Schematic diagram of the intensity balanced Sagnac interferometer photothermal deflection spectroscopy with a $CaCO_3$ birefringent crystal. The $CaCO_3$ crystal was inserted before the Sagnac interferometer. The beam diameter was 1.4 mm at the lens and the lateral distance between the two beams was about 2 mm.

2.3. Materials

Eu^{2+}-doped $CaAlSiN_3$ (CASN:Eu^{2+}) is a red phosphor with high quantum efficiency used for a white-light emitting diode (LED). We used CASN:Eu^{2+} powder with 1 mol% Eu and particle size of 17 μm. The PL/PLES spectrum and the quantum efficiency were measured using an absolute quantum efficiency measurement system (QE2000, Otsuka Electronics, Osaka, Japan). Internal quantum efficiency was measured to be 90%. The PTES was measured by the method 2 on the conditions described above as follows. CASN:Eu^{2+} powder was mounted and glued on a glass slide as a sample. The PTES spectrum was measured in the air. The modulation frequency of the pump was 20 Hz, and maximum excitation light intensity was 5 mW/ cm^2 @ 470 nm (210 μmol m^{-2}·s^{-1}). For normalization of the signal spectrum, activated carbon was put on the same slide and measured absolutely in the same manner. Then the raw photothermal spectrum of CASN:Eu^{2+} powder was divided by that of activated carbon to obtain the PTES of CASN:Eu^{2+}.

3. Results and Discussion

3.1. Results and Discussion 1

The average noise intensity was evaluated to be 152 and 81 without and with balanced detection, respectively, from the measurement data points between 400 nm and 697.5 nm (Figure 3). The S/N was improved by 1.8 times with the balanced detection.

The probe laser beam noise contributed about 90% out of the total noise size estimated by the measurement [11]. If the probe beam noise was completely removed, the S/N should be improved by about 10 times. Therefore, this optical system was not enough to subtract the probe laser beam noise. This insufficient S/N improvement was due to mismatch of the interference intensity at each photodiode. If the signal beam and reference beam were completely parallel, the interference light intensity of the signal beam coincides with that of the reference beam due to the optical common path. In this optical system, the signal beam and reference beam were split by the BS and one of the beams was reflected at the mirror before the Sagnac interferometer. Therefore, it was difficult to make these two beams parallel since the mirror before the Sagnac interferometer set in a non-common path

configuration. This problem was solved by the method 2 using a birefringence crystal, the result of which was explained in the following subsection.

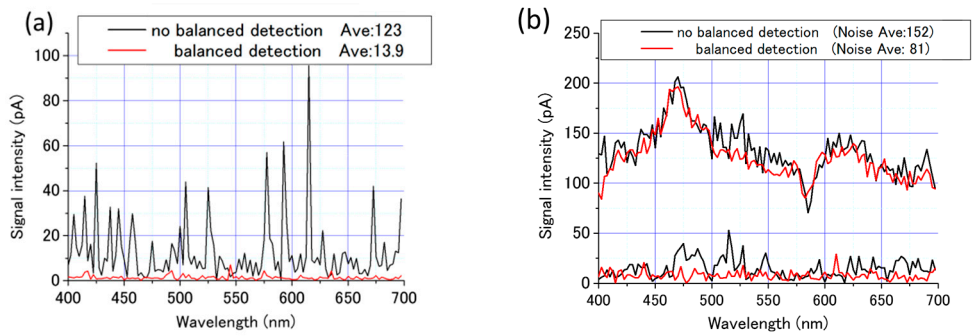

Figure 3. Measurement results of balanced detection for activated carbon in air as a deflection medium on lock-in detection condition with alternating current (AC) gain: 0 dB, Sensitivity: 1 nA, Time Constant: 5 s, and Modulation Frequency: 20 Hz. (**a**) measured only with the probe laser beam with the BS inserted after the Sagnac interferometer without excitation. (**b**) measured with the optical system in Figure 1.

3.2. Results and Discussion 2

Further improvement in the S/N value was demonstrated by the intensity balanced detection system with using a birefringent crystal. As shown in Figure 4, by suppressing the probe laser beam intensity noise more effectively, the intensity balanced detection with the $CaCO_3$ crystal successfully increased the S/N by the factor of about 4.0 from the no balanced detection scheme. Generation of completely parallel beams was the most essential in this improvement. The average value of the noise intensity was decreased from 152 to 42. The experimental result with the $CaCO_3$ crystal indicated smaller noise intensity than without the $CaCO_3$ crystal. However, if the probe laser intensity noise was completely removed, the S/N should be improved by ten times. This insufficient S/N improvement suggested the other noise origin. A possible origin of this insufficient noise suppression is different paths between the signal and reference beam. If the signal and reference beams passed the different space, the probe laser beam may be suffered from the different fluctuation effect of the atmosphere on the optical path.

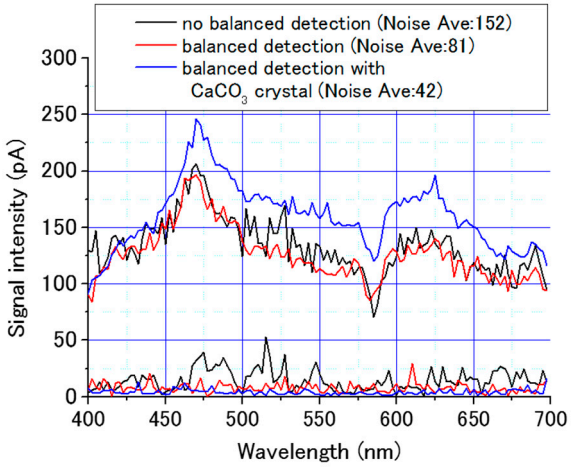

Figure 4. Measurement results of balanced detection with the $CaCO_3$ crystal for activated carbon in air as a deflection medium on lock-in detection condition with AC gain: 0 dB, Sensitivity: 1 nA, Time Constant: 5 s, and Modulation Frequency: 20 Hz. The balanced detection result with the $CaCO_3$ crystal (blue line) shows smaller averaged noise intensity than with the measurement results of no-balanced detection (black line) and balanced detection without the $CaCO_3$ crystal (red line).

The S/N for activated carbon was obtained to be more than 200 at the maximum excitation light intensity 5 mW/cm^2 @ 470 nm. Thus, the excitation light intensity required for S/N ≈ 12 is estimated to be 50 μW/cm^2.

3.3. Thermal Relaxation Spectrum

Using quasi-monochromatic light from a white-light lamp (Xe lamp, L11034, Hamamatsu Photonics, Shizuoka, Japan) as the excitation light, the PTES have been successfully obtained for CASN:Eu^{2+} powders [4] in the air as shown in Figure 5a, where photoluminescence (PL) and PLE spectra are also plotted.

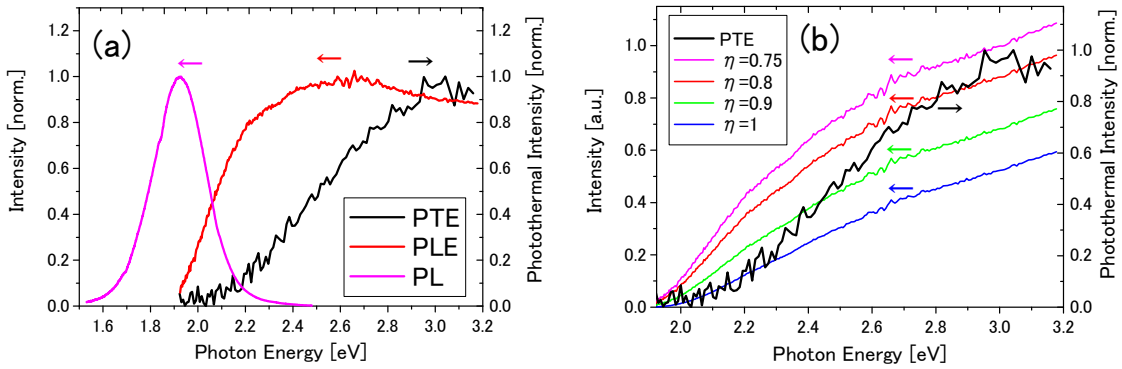

Figure 5. (**a**) Photothermal excitation, photoluminescence excitation, and photoluminescence spectra of Eu^{2+}-doped $CaAlSiN_3$ phosphors (CASN:Eu^{2+}). (**b**) Transformed photoluminescence excitation spectra with various luminescence quantum yields η compared with the photothermal excitation spectrum of CASN:Eu^{2+}. The photothermal excitation spectrum (PTES) is compared with the transformed photoluminescence excitation spectrum (PLES) expressed by $(E - 1.9\eta)/1.9\eta$ PLES(E).

Comparison of the PTES of CASN:Eu^{2+} with its PLES shows characteristic feature reflecting a high fluorescence quantum efficiency that the relative intensity of the PTES against the PLES decreases toward the absorption edge. In Figure 5b, in fact, the spectral shape of the PTES is reasonably reproduced by the PLES transformed with Equation (7) in Section 4, assuming that the absorbed light energy less than 1.9 eV (the peak energy of the PL spectrum) is converted into luminescence by 80 to 100% quantum efficiency and that the absorbed light energy exceeding 1.9 eV is all thermally relaxed to yield the photothermal signal. A theoretical discussion on the method how to transform PLES to reproduce PTES is undertaken in Section 4.

4. Relation Between Photothermal and Photoluminescence Excitation Spectra

Let us formulate the relation between PTES and PLES in terms of the luminescence quantum efficiency (or quantum yield) based on radiative transition in the conventional configurational coordinate model in the harmonic approximation as shown in Figure 6 [16]. We can reasonably assume a typical non-radiative relaxation process where rapid non-radiative relaxation occurs from the higher to lower excited states and from the vibrationally excited state into the bottom of the adiabatic potentials in the lowest excited state and in the ground state. It is assumed that the radiative transition occurs with the luminescence quantum efficiency (≤1) from the bottom of the adiabatic potential of the lowest excited state into the vibrationally excited levels in the adiabatic potential of the ground state.

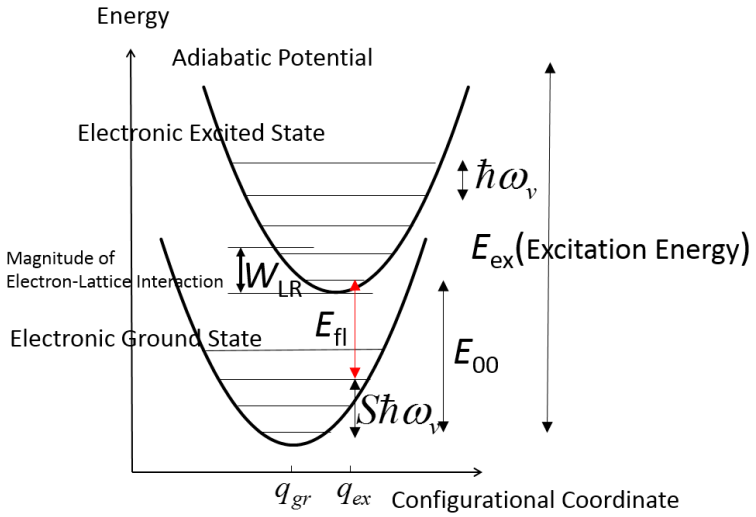

Figure 6. Radiative and non-radiative relaxation in the configurational coordinate model [16]. $\hbar\omega_v$: phonon energy, E_{00} : energy of zero phonon line, E_{fl} : fluorescence peak energy, q_{gr}, q_{ex} are the equilibrium configurations at electronic ground and excited states, respectively. W_{LR}: magnitude of electron-lattice interaction defined by the energy difference between the excited-state adiabatic potential energy at q_{gr} and that at q_{ex}.

As usual as depicted in Figure 6, we define the magnitude of electron-lattice interaction W_{LR} and phonon energy $\hbar\omega_v$ to obtain the Huang-Rhys factor S and the Franck–Condon factor F_{m0} as follows:

$$S = \frac{W_{LR}}{\hbar\omega_v},\ F_{m0} = \frac{e^{-S}S^m}{m!},\ \sum_m F_{m0} = 1,\ \text{and}\ \sum_m mF_{m0} = S \tag{1}$$

The conversion ratio P of excitation energy to thermal energy when luminescence quantum efficiency is 100% (assuming that relaxation within the adiabatic potential occurs non-radiatively):

$$P = \frac{E_{\mathrm{ex}} - E_{\mathrm{fl}}}{E_{\mathrm{ex}}} = \frac{E_{\mathrm{ex}} - (E_{00} - \sum_m m\hbar\omega_v F_{m0})}{E_{\mathrm{ex}}} \tag{2}$$

where E_{ex} is the excitation photon energy, E_{fl} is the fluorescence photon energy, and E_{00} is the zero phonon energy.

The photothermal excitation signal intensity (raw signal) $PTE(E_{\mathrm{ex}})$ is expressed by:

$$PTE(E_{\mathrm{ex}}) = \frac{E_{\mathrm{ex}} - \eta(E_{00} - S\hbar\omega_v)}{E_{\mathrm{ex}}}\beta(E_{\mathrm{ex}})n(E_{\mathrm{ex}})E_{\mathrm{ex}}\left(1 - e^{-\alpha_{\mathrm{ex}}L}\right), \tag{3}$$

where η is the luminescence quantum efficiency, $\beta(E_{\mathrm{ex}})$ is the spectral response function of the measurement apparatus, $n(E_{\mathrm{ex}})$ is the photon flux density of the excitation light, and α_{ex} is the absorption coefficient of the sample at E_{ex}.

Then, the photothermal excitation spectrum $PTES(E_{\mathrm{ex}})$ of the sample is obtained by normalizing $PTE(E_{\mathrm{ex}})$ with that of activated carbon ($\eta = 0,\ \alpha_{ex}L \gg 1$), $\beta n E_{\mathrm{ex}}$, as:

$$PTES(E_{\mathrm{ex}}) = \frac{E_{\mathrm{ex}} - \eta(E_{00} - S\hbar\omega_v)}{E_{\mathrm{ex}}}\left(1 - e^{-\alpha_{\mathrm{ex}}L}\right) = \frac{E_{\mathrm{ex}} - \eta E_{\mathrm{fl}}}{E_{\mathrm{ex}}}\left(1 - e^{-\alpha_{\mathrm{ex}}L}\right). \tag{4}$$

This equation shows PTES is proportional to the absorption spectrum (α_{ex}) if $\eta = 0$ and $\alpha_{ex}L \ll 1$.

The raw signal intensity for the photoluminescence excitation spectrum is expressed by:

$$PLE(E_{\mathrm{ex}}) = \frac{\eta(E_{00} - S\hbar\omega_v)}{E_{\mathrm{ex}}}\beta(E_{\mathrm{ex}})n(E_{\mathrm{ex}})E_{\mathrm{ex}}\left(1 - e^{-\alpha_{\mathrm{ex}}L}\right) = \frac{\eta E_{\mathrm{fl}}}{E_{\mathrm{ex}}}\beta n E_{\mathrm{ex}}\left(1 - e^{-\alpha_{\mathrm{ex}}L}\right), \tag{5}$$

which is normalized by $\beta n E_{\mathrm{ex}}$ to give the photoluminescence excitation spectrum:

$$PLES(E_{\mathrm{ex}}) = \frac{\eta E_{\mathrm{fl}}}{E_{\mathrm{ex}}}\left(1 - e^{-\alpha_{\mathrm{ex}} L}\right) \tag{6}$$

Thus, we finally obtain the relation between $PTES(E_{\mathrm{ex}})$ and $PLES(E_{\mathrm{ex}})$ as:

$$PTES(E_{\mathrm{ex}}) = \frac{E_{\mathrm{ex}} - \eta E_{\mathrm{fl}}}{\eta E_{\mathrm{fl}}} PLES(E_{\mathrm{ex}}) \tag{7}$$

In Figure 5, we assumed $\eta = 0.75,\ 0.8,\ 0.9,\ 1$ and $E_{\mathrm{fl}} = E_{00} - S\hbar\omega_v = 1.9\mathrm{eV}$ (the peak of the photoluminescence spectrum).

The PTES agrees with the transformed PLES within $\eta = 0.8$ to 1, consistent with $\eta = 0.9$ independently measured with the absolute quantum efficiency measurement system. Even though agreement is fairly good, there is evident residual difference. Possible reasons for the discrepancy are as follows.

Firstly, thermoluminescence from CASN:Eu^{2+} may distort PLES and/or PTES, causing departure from ideal behavior expected in the standard energy relaxation model. CASN:Eu^{2+} is known not only for high quantum efficiency but also for excellent thermal-quenching behavior. The mechanism of the latter nature is studied [17,18] and it is revealed that photoexcited electrons are partially trapped at trapping sites and thermally excited to yield thermoluminescence. This may also affect apparent luminescence quantum efficiency.

Secondly, it can be interpreted at face value, i.e., the luminescence quantum efficiency η depends on the excitation light energy as follows:

$$PTES(E_{ex}) = \frac{E_{ex} - \eta(E_{ex}) E_{fl}}{\eta(E_{ex}) E_{fl}} PLES(E_{ex}) \tag{8}$$

For example, if $\eta(E_{ex}) = 1 - 0.2\left(E_{ex} - E_{fl}\right)$, we obtain excellent agreement as shown in Figure 7. In fact, calculation of absorption spectrum of CASN:Eu^{2+} [19] shows that absorption increases monotonically up to 3.6 eV, inconsistent with the PLES presently observed, where the absorption levels off around 2.5 eV and decreases above 2.6 eV. This may be indicative of the onset of a non-radiative channel by higher energy excitation, such as intersystem crossing into the radiatively inactive triplet state. Therefore, it is reasonable for the luminescence quantum efficiency tends to decrease with energy as assumed in Figure 7. The other possibility is that $\alpha_{ex} L$ increases with photon energy to be in the absorption saturation region ($1 - e^{-\alpha_{ex} L} \approx 1$) above 2.6 eV. It is usually difficult to judge which is the case, but the improved agreement between the PTES and the transformed PLES in Figure 7 supports the former case. In order for the comparison between PTES and PLES to be valid, it is not necessary that the PLES is proportional to the absorption spectrum since the PTES and PLES have the same $(1 - e^{-\alpha_{ex} L})$ dependence.

Thirdly, excitation and observation geometry was not the same between PTES and PLES. In order to estimate the effect of geometry, we measured PLES in the geometry similar to PTES to find that almost the same PLES as shown in Figure 5 was obtained. However, we need further to consider the effect of possible difference between the optical and thermal thickness of the sample as discussed in Reference [20]. Therefore, we derive a more rigorous formula by taking these effects into account below.

When the incident photon flux density is n_0 at $E = E_{\mathrm{ex}}$, the photon flux $n_{\mathrm{p,ex}}$ at x (the depth from the surface), the density of the highest photoexcited state n_{ex}, the density of the lowest relaxed excited state n_{fl} (initial state of luminescence), flux density of luminescent photon $n_{\mathrm{p,fl}}$, and flux density of photon which is converted to emitted heat $n_{\mathrm{p,t}}$ obey the equations:

$$\frac{dn_{\mathrm{p,ex}}}{dx} = \alpha_{\mathrm{ex}} n_{\mathrm{p,ex}} \tag{9}$$

$$\frac{dn_{ex}}{dt} = \alpha_{ex} n_{p,ex} - \frac{n_{ex}}{\tau_{ex}} \tag{10}$$

$$\frac{dn_{fl}}{dt} = \frac{n_{ex}}{\tau_{ex}} - \frac{n_{fl}}{\tau_{fl}} - \frac{n_{fl}}{\tau_t} \tag{11}$$

$$n_{p,fl} = \int_0^L \frac{n_{fl}}{\tau_{fl}} e^{-\alpha_{fl} x} dx \tag{12}$$

$$n_{p,t} = \int_0^L \frac{n_{fl}}{\tau_t} e^{-\alpha_t x} dx \tag{13}$$

respectively, where α_{ex} and α_{fl} are the absorption coefficients at $E = E_{ex}$ and $E = E_{fl}$, α_t is the reciprocal of the thermal diffusion length, and τ_{ex}, τ_{fl}, and τ_t are the non-radiative decay time from the highest photoexcited state, radiative and non-radiative decay times from the lowest relaxed excited state, respectively. The luminescence quantum efficiency is given by:

$$\eta = \frac{1}{\tau_{fl}} / \left(\frac{1}{\tau_{fl}} + \frac{1}{\tau_t} \right). \tag{14}$$

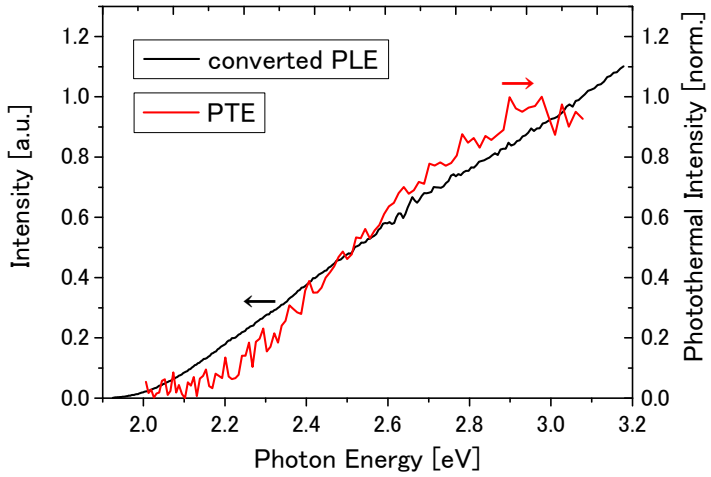

Figure 7. The PTES is compared with the transformed PLES expressed by $\frac{E-1.9\eta(E)}{1.9\eta(E)} PLES(E)$ with $\eta(E) = 1 - 0.2(E - 1.9)$.

The steady-state solutions for n_{ex} and n_{fl} are $n_{ex} = \tau_{ex}\alpha_{ex} n_0 e^{-\alpha_{ex} x}$ and $n_{fl} = \frac{1}{\frac{1}{\tau_{fl}} + \frac{1}{\tau_t}} \alpha_{ex} n_0 e^{-\alpha_{ex} x}$. Thus, luminescence photon flux density is given by:

$$n_{p,fl} = \frac{\frac{1}{\tau_{fl}}}{\frac{1}{\tau_{fl}} + \frac{1}{\tau_t}} \alpha_{ex} n_0 \frac{1 - e^{-(\alpha_{ex} + \alpha_{fl})L}}{\alpha_{ex} + \alpha_{fl}} = \eta \alpha_{ex} n_0 \frac{1 - e^{-(\alpha_{ex} + \alpha_{fl})L}}{\alpha_{ex} + \alpha_{fl}} \tag{15}$$

and photon flux which is converted to heat and emitted from the sample surface is:

$$n_{p,t} = \frac{\frac{1}{\tau_t}}{\frac{1}{\tau_{fl}} + \frac{1}{\tau_t}} \alpha_{ex} n_0 \frac{1 - e^{-(\alpha_{ex} + \alpha_t)L}}{\alpha_{ex} + \alpha_t} = (1 - \eta) \alpha_{ex} n_0 \frac{1 - e^{-(\alpha_{ex} + \alpha_t)L}}{\alpha_{ex} + \alpha_t} \tag{16}$$

The raw photothermal excitation signal is:

$$PTE = [(E_{ex} - E_{fl}) + E_{fl}(1 - \eta)] \alpha_{ex} n_0 \frac{1 - e^{-(\alpha_{ex} + \alpha_t)L}}{\alpha_{ex} + \alpha_t} \beta(E_{ex}) \tag{17}$$

Then, the photothermal excitation spectrum $PTES(E_{ex})$ of the sample is obtained by normalizing $PTE(E_{ex})$ with that of activated carbon $E_{ex}n_0\beta$ ($\eta = 0, \alpha_{ex}L \gg 1,\ \alpha_{ex} \gg \alpha_t$), as:

$$PTES(E_{ex}) = \frac{E_{ex} - \eta E_{fl}}{E_{ex}} \frac{\alpha_{ex}}{\alpha_{ex} + \alpha_t}\left(1 - e^{-(\alpha_{ex}+\alpha_t)L}\right). \tag{18}$$

(If $\eta = 0$, $\alpha_t L \gg 1$, and $\alpha_t \gg \alpha_{ex}$(thermally thick sample), then $PTES(E_{ex}) \propto \alpha_{ex}$. In this case, even if $\alpha_{ex}L \gg 1$, $PTES(E_{ex}) \propto \alpha_{ex}$ as discussed in Reference [20]).

The raw photoluminescence excitation signal is:

$$PLE = E_{fl}\eta\alpha_{ex}n_0 \frac{1 - e^{-(\alpha_{ex}+\alpha_{fl})L}}{\alpha_{ex} + \alpha_{fl}} \beta(E_{ex}) \tag{19}$$

which is normalized by $\beta n_0 E_{ex}$ (excitation light spectrum) to obtain:

$$PLES(E_{ex}) = \frac{\eta E_{fl}}{E_{ex}} \frac{\alpha_{ex}}{\alpha_{ex} + \alpha_{fl}}\left(1 - e^{-(\alpha_{ex}+\alpha_{fl})L}\right). \tag{20}$$

Thus, we finally obtain a more rigorous relation:

$$PTES(E_{ex}) = \frac{E_{ex} - \eta E_{fl}}{\eta E_{fl}} PLES(E_{ex}) \frac{1 - e^{-(\alpha_{ex}+\alpha_t)L}}{1 - e^{-(\alpha_{ex}+\alpha_{fl})L}} \frac{\alpha_{ex} + \alpha_{fl}}{\alpha_{ex} + \alpha_t} \tag{21}$$

If it is assumed that $\alpha_{fl}L \ll 1$ and $\alpha_t L \ll 1$, we again obtain the simple relation between $PTES(E_{ex})$ and $PLES(E_{ex})$ as:

$$PTES(E_{ex}) = \frac{E_{ex} - \eta E_{fl}}{\eta E_{fl}} PLES(E_{ex}) \tag{22}$$

In the present experiment, it is a good approximation that $\alpha_{fl} \ll \alpha_{ex}$ and $\alpha_{fl}L \ll 1$, so:

$$PTES(E_{ex}) = \frac{E_{ex} - \eta E_{fl}}{\eta E_{fl}} PLES(E_{ex}) \frac{1 - e^{-(\alpha_{ex}+\alpha_t)L}}{1 - e^{-\alpha_{ex}L}} \frac{\alpha_{ex}}{\alpha_{ex} + \alpha_t} \tag{23}$$

The absorption coefficient of $CaAlSiN_3$ is calculated to amount to 10^4 cm^{-1} in the visible, so that $e^{-\alpha_{ex}L} \approx 0$ is satisfied since the CASN:Eu^{2+} particles are >10 μm in diameter [19,21].

There is no literature available for α_t of CASN:Eu^{2+}, the reciprocal of thermal diffusion length which is a function of thermal diffusivity and modulation frequency of the excitation light. Thermal diffusivity is given by thermal conductivity/(density × specific heat). For CASN:Eu^{2+}, thermal conductivity (4 W m^{-1}·K^{-1}) and density (3.15 g·cm^{-1}) are measured in Reference [22], but specific heat is not known. From thermal diffusivity of similar phosphor ceramic material is given in Reference [23] and that of typical ceramics in Wikipedia [24], we can safely take 1 to 10 mm^2/s. Then, thermal diffusion length at f = 20 Hz is estimated to be 0.1 to 0.4 mm from (2 × thermal diffusivity/$2\pi f$)$^{1/2}$. Therefore, the sample is thermally thin ($\alpha_t L \ll 1$) considering the particle size, and $\alpha_{ex}\left(10^4\ cm^{-1}\right) \gg \alpha_t\left(10 - 100\ cm^{-1}\right)$. Consequently, the Equation (22) holds as a good approximation.

5. Conclusions

SIPDS was improved fourfold in S/N by implementing balanced detection scheme. For balanced detection in SIPDS, it is crucial to obtain the equivalent interference pattern at the two detectors for signal and reference. For this purpose, the method to generate completely parallel beams was devised with the use of a birefringent crystal calcite. The method was applied to evaluate luminescence quantum efficiency η of CASN:Eu^{2+}, well known red phosphor of white LED. We derived the relation between PTES and PLES, and proposed the method to estimate η by comparing the spectral shapes of PTES and PLES. The estimated value agrees well with that measured independently by the conventional absolute quantum efficiency measurement method. In addition, the agreement is improved if the

excitation energy dependent quantum efficiency (decreasing with energy) is assumed. However, since CASN:Eu^{2+} is a material showing persistent luminescence, the present formula relating PLES and PTES may not apply, requiring a more detailed analysis. One of the future, promising targets of the presently proposed method for estimating the excitation energy conversion efficiency is photosynthesis using live leaves. In order to estimate true solar energy conversion efficiency in photosynthesis by avoiding non-photochemical quenching, the excitation intensity is required to be well below 5 mW/cm^2. Quantum efficiency measurement of plants at such a weak excitation is within the scope of SIPDS availability.

Author Contributions: Conceptualization, E.T.; methodology, N.S., K.S., and E.T.; data analysis, E.T., N.S, and H.C.; investigation, H.C. and N.S.; sample synthesis and measurement of PL/PLES andη, K.T. and N.H.; writing—original draft preparation, E.T. and N.S.; writing—review and editing, E.T. and T.K.; supervision, E.T.; project administration, E.T.; funding acquisition, E.T. and N.S. All authors have read and agreed to the published version of the manuscript.

Funding: This research was partly funded by Ichimura Foundation for New Technology.

Conflicts of Interest: The authors declare no conflict of interest.

References

1. Ishida, H.; Tobita, S.; Hasegawa, Y.; Katoh, R.; Nozaki, K. Recent advances in instrumentation for absolute emission quantum yield measurements. *Coord. Chem. Rev.* **2010**, *254*, 2449–2458. [CrossRef]
2. Lahmann, W.; Ludewig, H.J. Opto—Acoustic determination of absolute quantum yields in flourescent solutions. *Chem. Phys. Lett.* **1977**, *45*, 177–179. [CrossRef]
3. Sugitani, Y.; Kato, K. Simultaneous Measurement of Photoacoustic and Excitation Spectra for the Evaluation of Quantum Efficiencies of Uranium-mica Type Compounds. *BCSJ* **1979**, *52*, 3499–3502. [CrossRef]
4. Kato, K.; Sugitani, Y. Cell Design for Simultaneous Measurement of Photoacoustic and Fluorescence Spectra. *BCSJ* **1979**, *52*, 3733–3734. [CrossRef]
5. Cahen, D.; Malkin, S.; Lerner, E.I. Photoacoustic spectroscopy of chloroplast membranes; listening to photosynthesis. *FEBS Lett.* **1978**, *91*, 339–342. [CrossRef]
6. Poulet, P.; Cahen, D.; Malkin, S. Photoacoustic detection of photosynthetic oxygen evolution from leaves. Quantitative analysis by phase and amplitude measurements. *Biochim. Biophys. Acta-Bioenerg.* **1983**, *724*, 433–446. [CrossRef]
7. Terazima, M.; Kanno, H.; Azumi, T. Measurement of the quantum yield of triplet formation (φISC) in a polymer matrix by the time-resolved thermal lens method: Excitation wavelength dependence of φISC of N-methyl-p-nitroaniline. *Chem. Phys. Lett.* **1990**, *173*, 327–330. [CrossRef]
8. Müller, P.; Li, X.-P.; Niyogi, K.K. Non-Photochemical Quenching. A Response to Excess Light Energy. *Plant Physiol.* **2001**, *125*, 1558–1566. [CrossRef]
9. Wu, J.; Kitamori, T.; Sawada, T. Ultramicrospectrochemical analysis and trace determination of compounds adsorbed on a single microparticulate sample by the optical beam deflection method. *Anal. Chem.* **1991**, *63*, 217–219. [CrossRef]
10. Shiokawa, N.; Mizuno, Y.; Tsuchiya, H.; Tokunaga, E. Sagnac interferometer for photothermal deflection spectroscopy. *Opt. Lett.* **2012**, *37*, 2655–2657. [CrossRef]
11. Shiokawa, N.; Tokunaga, E. Quasi first-order Hermite Gaussian beam for enhanced sensitivity in Sagnac interferometer photothermal deflection spectroscopy. *Opt. Express* **2016**, *24*, 11961–11974. [CrossRef] [PubMed]
12. Boccara, A.C.; Fournier, D.; Badoz, J. Thermo-optical spectroscopy: Detection by the "mirage effect". *Appl. Phys. Lett.* **1980**, *36*, 130–132. [CrossRef]
13. Uheda, K.; Hirosaki, N.; Yamamoto, Y.; Naito, A.; Nakajima, T.; Yamamoto, H. Luminescence Properties of a Red Phosphor, CaAlSiN3: Eu2 +, for White Light-Emitting Diodes. *Electrochem. Solid-State Lett.* **2006**, *9*, H22–H25. [CrossRef]
14. Xie, R.-J.; Hirosaki, N.; Takeda, T. Wide Color Gamut Backlight for Liquid Crystal Displays Using Three-Band Phosphor-Converted White Light-Emitting Diodes. *Appl. Phys. Express* **2009**, *2*, 022401. [CrossRef]

15. Ohkubo, K.; Nakagawa, Y. Quantum Efficiency Measurement of Lamp Phosphors in Accordance with Radiometric Standards. *J. Light Vis. Environ.* **2013**, *37*, 16–27. [CrossRef]
16. Henderson, B.; Imbusch, G.F. *Optical Spectroscopy of Inorganic Solids*; Clarendon/Oxford University Press: Oxford, UK, 2006; ISBN 978-0-19-929862-4.
17. Wang, J.; Zhang, H.; Lei, B.; Xia, Z.; Dong, H.; Liu, Y.; Zheng, M.; Xiao, Y. Enhanced photoluminescence and phosphorescence properties of red CaAlSiN 3:Eu 2+ phosphor via simultaneous UV-NIR stimulation. *J. Mater. Chem. C* **2015**, *3*, 4445–4451. [CrossRef]
18. Ueda, J.; Tanabe, S.; Takahashi, K.; Takeda, T.; Hirosaki, N. Thermal Quenching Mechanism of CaAlSiN3:Eu2+ Red Phosphor. *BCSJ* **2017**, *91*, 173–177. [CrossRef]
19. Jang, S.; Im, J.; Keuk Bang, B.; Hae Kim, C.; Chang, H.; Kong, K. First-principles calculation of metal-doped CaAlSiN 3: Material design for new phosphors. *RSC Adv.* **2015**, *5*, 39319–39323. [CrossRef]
20. Rosencwaig, A.; Gersho, A. Theory of the photoacoustic effect with solids. *J. Appl. Phys.* **1976**, *47*, 64–69. [CrossRef]
21. Wang, Z.; Shen, B.; Dong, F.; Wang, S.; Su, W.-S. A first-principles study of the electronic structure and mechanical and optical properties of CaAlSiN 3. *Phys. Chem. Chem. Phys.* **2015**, *17*, 15065–15070. [CrossRef]
22. Li, S.; Zhu, Q.; Wang, L.; Tang, D.; Cho, Y.; Liu, X.; Hirosaki, N.; Nishimura, T.; Sekiguchi, T.; Huang, Z.; et al. CaAlSiN 3:Eu 2+ translucent ceramic: A promising robust and efficient red color converter for solid state laser displays and lighting. *J. Mater. Chem. C* **2016**, *4*, 8197–8205. [CrossRef]
23. Yoon, H.C.; Yoshihiro, K.; Yoo, H.; Lee, S.W.; Oh, J.H.; Do, Y.R. Low-Yellowing Phosphor-in-Glass for High-Power Chip-on-board White LEDs by Optimizing a Low-Melting Sn-P-F-O Glass Matrix. *Sci. Rep.* **2018**, *8*, 1–11. [CrossRef] [PubMed]
24. Thermal diffusivity. Wikipedia, 2019. Available online: https://en.wikipedia.org/wiki/Thermal_diffusivity (accessed on 26 December 2019).